Mixed-Valence Biferrocenes: Pronounced Anion Dependence of Valence Detrapping and Effects of an Asymmetric Crystal Lattice

Robert J. Webb,[1,2] Steven J. Geib,[3] Donna L. Staley,[3] Arnold L. Rheingold,*[,3] and David N. Hendrickson*[,1]

Contribution from the Department of Chemistry, D-006, University of California at San Diego, La Jolla, California 92093-0506, School of Chemical Sciences, University of Illinois, Urbana, Illinois 61801, and the Department of Chemistry, University of Delaware, Newark, Delaware 19716. *Received December 11, 1989*

Abstract: The effect of changing the anion from I_3^- to either PF_6^- or SbF_6^- upon the rate of intramolecular electron transfer in salts of the mixed-valence 1′,1‴-dibenzylbiferrocenium cation is investigated. Single-crystal X-ray structures are presented for 1′,1‴-dibenzylbiferrocene (**1**), 1′,1‴-dibenzylbiferrocenium hexafluorophosphate (**2**), and 1′,1‴-dibenzylbiferrocenium hexafluoroantimonate (**3**). Complex **1** crystallizes at 296 K in the monoclinic space group $P2_1/c$ with a unit cell of a = 5.846 (1) Å, b = 25.878 (7) Å, c = 8.354 (2) Å, and β = 93.73 (2)° with Z = 2. Refinement was carried out with 1862 (5.0σ) observed reflections to give R = 0.0353 and R_w = 0.0383. A center of symmetry (planar fulvalenide ligand) and a trans conformation characterize the Fe_2^{II} molecule in **1**. The PF_6^- salt **2** crystallizes at 296 K in the monoclinic space group $C2/c$ with a unit cell of a = 14.640 (2) Å, b = 12.938 (2) Å, c = 15.463 (3) Å and β = 93.70 (1)° with Z = 4. Refinement was carried out with 2139 (5.0σ) observed reflections to give R = 0.0483 and R_w = 0.0545. The PF_6^- anion was found to be disordered in two positions, one with an occupancy of 64% and the other 36%. Since the mixed-valence 1′,1‴-dibenzylbiferrocenium cation sits on a center of symmetry, the dihedral angle for the fulvalenide ligand is 0°. The two crystallographically equivalent metallocene moieties in the cation of **2** have dimensions intermediate between those of Fe^{II} and Fe^{III} metallocenes. The packing in complex **2** is that of layers of mixed-valence cations with the small PF_6^- anions sandwiched between the layers. 1′,1‴-Dibenzylbiferrocenium hexafluoroantimonate (**3**) crystallizes in the monoclinic space group $P2_1$, which at 198 K has a unit cell of a = 10.850 (2) Å, b = 11.874 (3) Å, c = 11.990 (6) Å, and β = 103.03 (2)° with Z = 2 and at 298 K has a unit cell of a = 10.899 (2) Å, b = 11.969 (3) Å, c = 12.145 (5) Å, and β = 102.88 (2)° with Z = 2. The refinements were carried out with 2568 (2.58σ) and 1955 (2.58σ) observed reflections at 198 and 298 K, respectively, to give R = 0.034 and R_w = 0.042 at 198 K and R = 0.039 and R_w = 0.047 at 298 K. The SbF_6^- anion in complex **3** was not found to be disordered at either temperature; however, at 298 K the thermal parameters for this anion are large. The mixed-valence cation has a trans conformation where the fulvalenide dihedral angle is 6.81° at 298 K and 7.01° at 198 K. The dimensions of the two halves of the mixed-valence cation in complex **3** are different. The positioning of the SbF_6^- anion relative to the nearest cation is not symmetric. At 298 K one Fe···Sb distance is 5.471 (3) Å, whereas the other one is 5.833 (4) Å. For the mixed-valence cation of SbF_6^- salt **3** there is a driving force to make one iron ion Fe^{III} and the other Fe^{II} due to the positioning of the SbF_6^- anion. The ^{57}Fe Mössbauer spectrum of PF_6^- complex **2** shows that the mixed-valence cation in this salt begins to become valence detrapped above ~100 K, and by 170 K the cation is valence detrapped on the Mössbauer time scale. This is contrasted to the case of 1′,1‴-dibenzylbiferrocenium triiodide which was reported to valence detrap at 270 K. For the SbF_6^- complex **3** Mössbauer data show an onset of valence detrapping in the 120–150 K range, and above ~200–250 K this complex is completely valence detrapped. An analysis of the temperature dependence of the spectral areas of the Mössbauer signals indicates that the PF_6^- and SbF_6^- anions are probably converting from static to dynamic in the temperature region where the mixed-valence cations in complexes **2** and **3** are becoming valence detrapped. The room-temperature IR spectrum for SbF_6^- complex **3** shows ⊥ C–H bending vibrational bands for both Fe^{II} and Fe^{III} metallocene units. Thus, there is at all temperatures a potential-energy barrier for electron transfer. At 7 K complex **3** gives an axial EPR spectrum with $g_\parallel$ = 3.35 and $g_\perp$ = 1.86. This signal broadens with increasing temperature and disappears above ~150 K. A similar axial signal is seen at low temperatures for complex **2**, but upon heating **2** this signal is replaced by a single derivative at g = 2.00, which persists up to at least 295 K. The origin of this difference in EPR characteristics between **2** and **3** is discussed. The nature of the appreciable anion influence on rate of intramolecular electron transfer is described as is the mechanism by which the mixed-valence cation in SbF_6^- complex **3** valence detraps even though it is sitting in such an asymmetric lattice site. The potential significance of these environmental effects on rates of electron transfer is highlighted in reference to solution redox processes.

The environment about a donor–acceptor pair in an electron-transfer event may play a crucial role in determining the rate of electron transfer. It has been suggested,[4] for example, that the motion of one or more amino acid moieties at a rate of 10^2–10^4 s^{-1} in a region near to the heme in cytochrome-c modulates the rate of electron transfer into or out of the redox site of this important respiratory electron transport protein. The discussion about whether slow reorganization of the immediate solvent structure affects the rate of outer-sphere electron transfer between transition-metal complexes in solution is ongoing.[5] In this same vein it is possible that an anion associated with an outer-sphere precursor complex moves so slowly that it affects the rate of electron transfer. Recently it has been noted[6] that aggregation of an anion with a cationic binuclear mixed-valence complex in solution affects the NIR intervalence-transfer (IT) electronic absorption band and, presumably, the rate of intramolecular electron transfer. In addition, it also has been found[7] that pressure freezing of solutions of mixed-valence complexes does not shift the IT band nearly as dramatically as is predicted by a dielectric continuum model. This means that the immediate solvent structure about a mixed-valence complex in solution may be less mobile than originally believed. Furthermore, we have found[8]

(1) University of California at San Diego.
(2) University of Illinois.
(3) University of Delaware.
(4) Williams, G.; Moore, G. R.; Williams, R. J. P. *Comments Inorg. Chem.* **1985**, *4*, 55–98.
(5) Only a few recent references are given: (a) Jortner, J.; Bixon, M. *J. Chem. Phys.* **1988**, *88*, 167–170. (b) Rips, I.; Jortner, J. *J. Chem. Phys.* **1987**, *87*, 2090–2104. (c) Hynes, J. T. *J. Phys. Chem.* **1986**, *90*, 3701–3706. (d) Kjaer, A. M.; Ulstrup, J. *Inorg. Chem.* **1986**, *25*, 644–651. (e) Haim, A. *Comments Inorg. Chem.* **1985**, *4*, 113–149.
(6) Lowery, M. D.; Hammack, W. S.; Drickamer, H. G.; Hendrickson, D. N. *J. Am. Chem. Soc.* **1987**, *109*, 8019–8024.
(7) (a) Hammack, W. S.; Drickamer, H. G.; Lowery, M. D.; Hendrickson, D. N. *Chem. Phys. Lett.* **1986**, *132*, 231–235. (b) Hammack, W. S.; Drickamer, H. G.; Lowery, M. D.; Hendrickson, D. N. *Inorg. Chem.* **1988**, *27*, 1307–1308. (c) Lewis, N. A.; Obeng, Y. S. *J Am. Chem. Soc.* **1988**, *110*, 2706.

0002-7863/90/1512-5031$02.50/0

the conversion from static to dynamic of the solvate molecules (S) near to the mixed-valence complex in crystals of $[Fe_3O(O_2CCH_3)_6(py)_3]\cdot S$ appreciably affects the rate of intramolecular electron transfer in the $Fe_2^{III}Fe^{II}$ complex.

In the last few years there has been considerable progress made in understanding what factors control the rate of intramolecular electron transfer in the *solid state* for mixed-valence trinuclear iron acetates[8] and biferrocenes.[9] In the case of mixed-valence biferrocenes the only salts which have been studied in any detail are the trihalide salts, where I_3^-, $BrIBr^-$, etc., have been employed as the anion. In a series of I_3^- salts of various disubstituted biferrocenium cations compounds have exhibited three different types of temperature dependencies. There are those which are valence trapped at all temperatures, those which are valence detrapped at all temperatures, and those which convert from valence trapped at low temperature to valence detrapped at some higher temperatures.

In this paper we report the effects of changing the anion from I_3^- to either PF_6^- or SbF_6^- upon the temperature of valence detrapping for the mixed-valence 1′,1‴-dibenzylbiferrocenium cation. Single-crystal X-ray structures and considerable physical data are presented for 1′,1‴-dibenzylbiferrocene (**1**) and the PF_6^- (**2**) and SbF_6^- (**3**) salts of the mixed-valence 1′,1‴-dibenzylbiferrocenium cation. An interesting observation is made for the SbF_6^- salt. The 298 K X-ray structural results show two crystallographically different iron ions in each cation. In spite of this, ^{57}Fe Mössbauer data show that the SbF_6^- valence detraps at ~200 K. Complex **3** is the first documented case of a mixed-valence complex with two crystallographically inequivalent metal ions which becomes detrapped as the temperature is increased.

Experimental Section

Compound Preparation. A sample of 1′,1‴-dibenzylbiferrocene was prepared according to literature methods[10] and identified by melting point and mass spectral data. 1′,1‴-Dibenzylbiferrocenium hexafluorophosphate, **2**, was made by oxidizing the neutral 1′,1‴-dibenzylbiferrocene dissolved in a minimum amount of benzene of dropwise adding a diethyl ether solution containing a stoichiometric amount of *p*-benzoquinone and HPF_6. The dark purple microcrystals were collected by filtration and washed with three portions of benzene and one portion of diethyl ether. The solid was dried in a dessicator overnight. 1′,1‴-Dibenzylbiferrocenium hexafluoroantimonate, **3**, was made in a similar manner. However, in this case, all of the reaction vessels were made of Nalgene because $HSbF_6$ etches glass. Anal. Calcd for 1′,1‴-dibenzylbiferrocenium hexafluorophosphate ($C_{34}H_{30}Fe_2PF_6$): C, 58.73; H, 4.32; Fe, 16.08. Found: C, 58.41; H, 4.23; Fe, 15.94. Anal. Calcd for 1′,1‴-dibenzylbiferrocenium hexafluoroantimonate ($C_{34}H_{30}Fe_2SbF_6$): C, 51.95; H, 3.82; Fe, 14.22. Found: C, 51.33; H, 3.90; Fe, 13.98.

Physical Methods. ^{57}Fe Mössbauer spectra were run on a constant-acceleration instrument which has been described previously.[11] We estimate the absolute temperature accuracy to be ±3 K; the relative precision is ±0.5 K. Mössbauer spectra were least-squares fit to Lorentzian line shapes with a previously documented computer program.[12] Isomer shifts values are given relative to iron foil at room temperature with no correction for second-order Doppler effects.

Variable-temperature X-band EPR spectra of polycrystalline samples were run on a Bruker ER 220D-SRC spectrometer equipped with an Air Products temperature controller. A calibrated copper-constantan thermocouple was used to determine the sample temperature.

Infrared spectra were obtained with a Nicolet Model MX-5 spectrometer. All samples were prepared as 13-mm KBr pellets with 2–5 mg of compound mixed well with 150 mg of KBr.

X-ray powder diffraction patterns were obtained on a Rigaku D/max powder diffractometer equipped with a copper X-ray tube, graphite monochromator, and variable-temperature liquid-nitrogen cold stage. The polycrystalline sample was spread evenly in silicone grease on a copper plate. The copper(111) reflection is seen in all of the patterns at ~43.3°.

X-ray Structure Determinations of 1′,1‴-Dibenzylbiferrocenium Hexafluoroantimonate (3). Diffraction data were collected on an Enraf-Nonius CAD4 automated k-axis diffractometer. The θ–2θ scan technique was used to record the intensities for all nonequivalent reflections. Scan widths were calculated as $A + B \tan \theta$, where A is estimated from the mosaicity of the crystal and B allows for the increase in peak width due to Mo $K_{\alpha 1}$–$K_{\alpha 2}$ splitting.

Data were collected for complex **3** at both 198 and 298 K. The dark purple, opaque platelike crystal used for data collection had well-developed faces except for the (1 0 1) face which was slightly damaged. There were a few small crystallites attached to the surface of the sample. The crystal was approximately bound by the following inversion related forms: (2 0 −1), (0 1 0), and (1 0 1). Distances from the crystal center to these facial boundaries were 0.03, 0.18, and 0.29 mm, respectively. The crystal was mounted with epoxy to a thin glass fiber with the (0 3 −5) scattering planes roughly normal to the spindle axis. Details of the data collection and structure refinement are given in Table I.

The 298 K structure was solved by direct methods (SHELXS-86); correct positions for the antimony and iron atoms were deduced from an E-map. Subsequent least-squares-difference Fourier calculations gave positions for the remaining non-hydrogen atoms. Hydrogen atoms were included as fixed contributors in "idealized" positions. In the final cycle of least squares, anisotropic thermal coefficients were refined for the non-hydrogen atoms and a group isotropic thermal parameter was varied for the hydrogen atoms. Successful convergence was indicated by the maximum shift/error for the last cycle. Refinement of the enantiomeric model significantly changed the weighted residual (R_w = 0.054). The final

Table I. Crystal Data for 1′,1‴-Dibenzylbiferrocenium Hexafluoroantimonate (**3**)

	298 K	198 K
formula	$C_{34}H_{30}Fe_2SbF_6$	
formula weight	786.05	
crystal system	monoclinic	monoclinic
space group	$P2_1$	$P2_1$
a, Å	10.899 (2)	10.850 (2)
b, Å	11.969 (3)	11.874 (3)
c, Å	12.145 (5)	11.990 (6)
β, deg	102.88 (2)	103.03 (2)
V, Å^3	1544 (1)	1505 (1)
Z	2	2
μ(Mo Kα), cm^{-1}	18.59	19.08
d(calcd), g/cm	1.691	1.734
color	dark purple	
size, mm	0.1 × 0.4 × 0.6	
scan limits, deg	1.50[1.00 + 0.35 tan (θ)] shell 1 2.0 < 2θ < 40.0	
scan mode	ω/θ	
octants collected	$\pm h,\gamma k,-l$	
T_{max}/T_{min}	1.799 empirical abs correction applied	
rflns collected	3405	3328
intensities processed	3179	3105
obs reflns, $I > 2.58\sigma(I_0)$	1955	2568
R, R_w, %	3.9, 4.7	3.4, 4.2
data/variable	5.04	6.62
final diff.	+0.38 > e/Å^3 > −0.39	+0.52 > e/Å^3 > −0.68
final shift/error	0.049	0.001

(8) (a) Jang, H. G.; Geib, S. J.; Kaneko, Y.; Nakano, M.; Sorai, M.; Rheingold, A. L.; Montez, B.; Hendrickson, D. N. *J. Am. Chem. Soc.* **1989**, *111*, 173. (b) Kaneko, Y.; Nakano, M.; Sorai, M.; Jang, H. G.; Hendrickson, D. N. *Inorg. Chem.* **1989**, *28*, 1067. (c) Oh, S. M.; Wilson, S. R.; Hendrickson, D. N. Woehler, S. E.; Wittebort, R. J.; Inniss, D.; Strouse, C. E. *J. Am. Chem. Soc.* **1987**, *109*, 1073. (d) Woehler, S. E.; Wittebort, R. J.; Oh, S. M.; Kambara, T.; Hendrickson, D. N.; Inniss, D.; Strouse, C. E. *J. Am. Chem. Soc.* **1987**, *109*, 1063. (e) Woehler, S. E.; Wittebort, R. J.; Oh, S. M.; Hendrickson, D. N.; Inniss, D.; Strouse, C. E. *J. Am. Chem. Soc.* **1986**, *108*, 2938. (f) Hendrickson, D. N.; Oh, S. M.; Dong, T.-Y.; Kambara, T.; Cohn, M. J.; Moore, M. F. *Comments Inorg. Chem.* **1985**, *4*, 329. (g) Sorai, M.; Kaji, K.; Hendrickson, D. N.; Oh, S. M. *J. Am. Chem. Soc.* **1986**, *108*, 702.

(9) (a) Dong, T.-Y.; Cohn, M. J.; Hendrickson, D. N.; Pierpont, C. G. *J. Am. Chem. Soc.* **1985**, *107*, 4777. (b) Cohn, M. J.; Dong, T.-Y.; Hendrickson, D. N.; Geib, S. J.; Rheingold, A. L. *J. Chem. Soc., Chem. Commun.* **1985**, 1095. (c) Dong, T.-Y.; Hendrickson, D. N.; Iwai, K.; Cohn, M. J.; Rheingold, A. L.; Sano, H.; Motoyama, I.; Nakashima, S. *J. Am. Chem. Soc.* **1985**, *107*, 7996. (d) Dong, T.-Y.; Hendrickson, D. N.; Pierpont, C. G.; Moore, M. F. *J. Am. Chem. Soc.* **1986**, *108*, 963. (e) Moore, M. F.; Wilson, S. R.; Cohn, M. J.; Dong, T.-Y.; Mueller-Westerhoff, U. T.; Hendrickson, D. N. *Inorg. Chem.* **1985**, *24*, 4559. (f) Dong, T.-Y.; Kambara, T.; Hendrickson, D. N. *J. Am. Chem. Soc.* **1986**, *108*, 4423. (g) Dong, T.-Y.; Kambara, T.; Hendrickson, D. N. *J. Am. Chem. Soc.* **1986**, *108*, 5857. (h) Sorai, M.; Nishimori, A.; Hendrickson, D. N.; Dong, T.-Y.; Cohn, M. J. *J. Am. Chem. Soc.* **1987**, *109*, 4266. (i) Kambara, T.; Hendrickson, D. N.; Dong, T.-Y.; Cohn, M. J. *J. Chem. Phys.* **1987**, *86*, 2362.

(10) Yamakawa, K.; Hisetome, M.; Sako, Y.; Ichida, S. *J. Organomet. Chem.* **1975**, *93*, 219.

(11) Cohn, M. J.; Timken, M. D.; Hendrickson, D. N. *J. Am. Chem. Soc.* **1984**, *106*, 6683.

(12) Chrisman, B. L.; Tumolillo, T. A. *Comput. Phys. Commun.* **1971**, *2*, 322.

Table II. Crystal Data for 1′,1‴-Dibenzylbiferrocene (**1**) and 1′,1‴-Dibenzylbiferrocenium Hexafluorophosphate (**2**)

	complex **1**	complex **2**
formula	$C_{34}H_{30}Fe_2$	$C_{34}H_{30}Fe_2PF_6$
formula weight	550.31	695.27
crystal system	monoclinic	monoclinic
space group	$P2_1/c$	$C2/c$
a, Å	5.846 (1)	14.640 (2)
b, Å	25.878 (7)	12.938 (2)
c, Å	8.354 (2)	15.463 (3)
β, deg	93.73 (2)	93.70 (1)
V, Å^3	759.0 (3)	2922.7 (8)
Z	2	4
μ(Mo Kα), cm^{-1}	11.71	11.07
d(calcd), g cm^{-3}	1.45	1.58
color	orange	black
size, mm	0.30 × 0.30 × 0.20	0.25 × 0.25 × 0.35
temp, K	296	296
scan limits, deg	4-55	4-55
scan mode	θ–2θ	θ–2θ
octants collected	$\pm h,+k,+l$	±20,+17,+21
T_{max}/T_{min}	1.18	1.081 Empirical abs correction
rflns collected	2722	3635
ind data (R_{int}, %)		3363 (1.67)
obs data, $F_o \geq 5\sigma$	1862	2139
R, R_w	0.035, 0.038	0.048, 0.054
GOF	1.055	1.241
data/parameter	8.8	7.8
$\Delta(\rho)_{max}$, e Å^{-3}	0.288	0.654
Δ/σ_{max}	0.090	0.070

difference Fourier map had no significant features. A final analysis of variance between observed and calculated structure factors showed no apparent systematic errors.

Refinement of a disordered model with three "idealized" octahedra (Sb–F, 1.89 Å) representing the SbF_6^- anion did not improve the fit of data ($R = 0.048$ and $R_w = 0.062$). Moreover, a comparison between the 298 and 198 K structures indicates that the change in temperature essentially only affects the thermal parameters.

No problems were encountered collecting the 198 K data, and there was no change in the appearance of the sample during the experiment. The crystal was mounted on a different goniometer head for collecting these data and the unit cell dimensions were redetermined. The a and c axes were inverted during the experiment but transformed to correspond to the room temperature setting for refinement.

The 198 K structure was solved by using atomic parameters from the room-temperature data. Hydrogen atoms were included as fixed contributors in "idealized" positions. In the final cycle of least-squares refinement, anisotropic thermal parameters were refined for the nonhydrogen atoms, and a group isotropic thermal parameter was varied for the hydrogen atoms. Successful convergence was indicated by the maximum shift/error for the last cycle. Refinement of the enantiomeric model significantly changed the weighted residual ($R_w = 0.049$). The final difference Fourier map had no significant features. A final analysis of variance between observed and calculated structure factors showed no apparent systematic errors.

X-ray Structure Determination of 1′,1‴-Dibenzylferrocenium Hexafluorophosphate (2) at 296 K. Diffraction data were collected on a Nicolet R3 diffractometer for complex **2** at 296 K. Details of the data collection and structure refinement are given in Table II. No evidence of crystal decomposition was noted. The unit cell parameters, listed in Table II, were obtained by a least-squares fit to the automatically centered settings of 25 reflections. The data were corrected for Lorentz, polarization, and anomalous dispersion effects. The data were also corrected empirically for absorption (max/min transm = 1.081).

The structure of **2** was solved by direct methods which located the Fe and P atoms; the remaining atoms were obtained from subsequent difference Fourier syntheses. Refinement was carried out by block-cascade methods. All non-hydrogen atoms were refined with anisotropic thermal parameters; isotropic parameters were used for the hydrogen atoms. The two phenyl rings of the cation were constrained to be rigid hexagons. The PF_6^- anion was found to be disordered in two positions (vide infra).

X-ray Structure Determination of 1′,1‴-Dibenzylbiferrocene (1) at 296 K. Diffraction data were collected on a Nicolet R3 diffractometer for complex **1** at 296 K. Details of the data collection and structure refinement are given in Table II. There was no evidence of crystal decomposition. The data were corrected for Lorentz, polarization, anomalous dispersion, and absorption effects.

Table III. Selected Bond Distances and Angles for 1′,1‴-Dibenzylbiferrocene (**1**) at 296 K

Distances			
Fe–C(1)	2.067 (3)	Fe–C(2)	2.045 (3)
Fe–C(3)	2.042 (3)	Fe–C(4)	2.037 (3)
Fe–C(5)	2.044 (3)	Fe–C(6)	2.052 (3)
Fe–C(7)	2.035 (3)	Fe–C(8)	2.046 (3)
Fe–C(9)	2.048 (3)	Fe–C(10)	2.058 (3)
C(1)–C(2)	1.427 (4)	C(1)–C(5)	1.426 (4)
C(1)–C(1A)	1.463 (6)	C(2)–C(3)	1.420 (5)
C(3)–C(4)	1.412 (5)	C(4)–C(5)	1.421 (5)
C(6)–C(7)	1.422 (4)	C(6)–C(10)	1.419 (4)
C(6)–C(11)	1.510 (5)	C(7)–C(8)	1.419 (5)
C(8)–C(9)	1.405 (5)	C(9)–C(10)	1.418 (4)
C(11)–C(17)	1.517 (4)		
Angles			
C(5)–C(1)–C(1A)	126.1 (3)	C(2)–C(1)–C(1A)	126.8 (3)
C(2)–C(3)–C(4)	107.8 (3)	C(1)–C(2)–C(3)	108.5 (3)
C(1)–C(5)–C(4)	108.0 (3)	C(3)–C(4)–C(5)	108.5 (3)
C(10)–C(6)–C(11)	126.5 (3)	C(7)–C(6)–C(10)	107.0 (3)
C(7)–C(8)–C(9)	107.4 (3)	C(7)–C(6)–C(11)	126.4 (3)
C(6)–C(10)–C(9)	108.1 (3)	C(6)–C(7)–C(8)	108.8 (3)
C(11)–C(17)–C(12)	120.4 (2)	C(8)–C(9)–C(10)	108.7 (3)
C(2)–C(1)–C(5)	107.2 (3)	C(6)–C(11)–C(17)	114.0 (3)
C(11)–C(17)–C(16)	119.6 (2)		

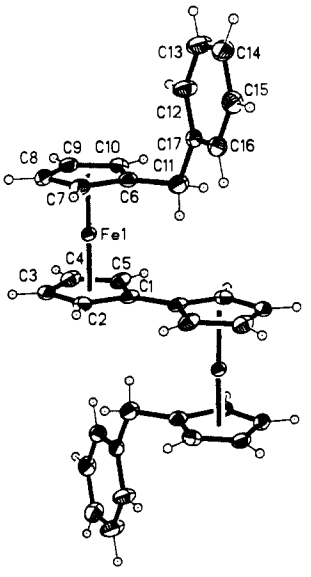

Figure 1. ORTEP drawing of 1′,1‴-dibenzylbiferrocene (**1**).

The structure of **1** was solved by direct methods, which located the Fe atom; the remaining atoms were obtained from subsequent difference Fourier syntheses. Refinement was carried out by block-cascade methods. The two phenyl rings were refined as rigid bodies.

Results

X-ray Structure Determination of 1′,1‴-Dibenzylbiferrocene (1). Complex **1** crystallizes in the monoclinic space group $P2_1/c$. Final positional parameters are available in the Supplementary Material; selected bond distances and angles are given in Table III. A perspective drawing of a molecule of 1′,1‴-dibenzylbiferrocene is given in Figure 1. Complex **1** sits on a center of symmetry. Average distances from the iron atoms to the ring carbon atoms are 2.048 (3) and 2.047 (3) Å to the benzylcyclopentadienyl and fulvalenide rings, respectively. These distances are closer to the value of 2.033 (10) Å found[13] for ferrocene than the value of 2.075 (10) Å found[14] for the ferrocenium cation. Distances from the iron atom to the centers-of-mass (COM) of the two rings are 1.652 (5) and 1.656 (5) Å where the shortest separation is to the fulvalenide ring. The ring COM-to-COM separation is 3.308 (10) Å.

(13) Seiler, P.; Dunitz, J. D. *Acta Crystallogr., Sect. B* **1979**, *35*, 1068.
(14) Mammano, N. J.; Zalkin, A.; Landers, A.; Rheingold, A. L. *Inorg. Chem.* **1977**, *16*, 297.

Table IV. Selected Bond Distances and Angles from the 198 and 298 K Structures of 1′,1‴-Dibenzylbiferrocenium Hexafluoroantimonate (**3**)

Distances

	198 K	298 K		198 K	298 K		198 K	298 K
Sb-F1	1.861 (6)	1.855 (9)	Sb-F2	1.869 (7)	1.82 (1)	Sb-F3	1.843 (8)	1.85 (1)
Sb-F4	1.869 (7)	1.85 (1)	Sb-F5	1.855 (7)	1.82 (1)	Sb-F6	1.854 (6)	1.84 (1)
Fe1-C1	2.081 (8)	2.08 (1)	Fe1-C2	2.060 (9)	2.04 (1)	C1-C2	1.40 (1)	1.39 (2)
Fe1-C3	2.038 (9)	2.06 (2)	C2-C3	1.40 (1)	1.40 (2)	Fe1-C4	2.057 (7)	2.05 (1)
C3-C4	1.41 (1)	1.42 (2)	Fe1-C5	2.140 (6)	2.143 (10)	C1-C5	1.43 (1)	1.41 (2)
C4-C5	1.43 (1)	1.43 (2)	Fe2-C6	2.044 (7)	2.04 (1)	C5-C6	1.40 (1)	1.42 (2)
Fe2-C7	2.038 (8)	2.04 (1)	C6-C7	1.42 (1)	1.45 (2)	Fe2-C8	2.038 (10)	2.04 (2)
C7-C8	1.41 (1)	1.38 (2)	Fe2-C9	2.043 (9)	2.04 (2)	C8-C9	1.42 (2)	1.40 (3)
Fe2-C10	2.034 (7)	2.02 (1)	C6-C10	1.46 (1)	1.43 (2)	C9-C10	1.43 (1)	1.44 (2)
Fe1-C11	2.084 (9)	2.08 (2)	Fe1-C12	2.089 (9)	2.10 (1)	C11-C12	1.42 (1)	1.42 (2)
Fe1-C13	2.085 (8)	2.06 (1)	C1-C13	1.39 (1)	1.36 (2)	Fe1-C14	2.070 (8)	2.06 (1)
C13-C14	1.41 (1)	1.44 (2)	Fe1-C15	2.065 (7)	2.08 (1)	C11-C15	1.41 (1)	1.42 (2)
C14-C15	1.40 (1)	1.38 (2)	C15-C16	1.52 (1)	1.48 (2)	C16-C17	1.51 (1)	1.53 (2)
C17-C18	1.36 (1)	1.34 (2)	C18-C19	1.40 (1)	1.43 (2)	C19-C20	1.37 (1)	1.34 (3)
C20-C21	1.35 (1)	1.36 (2)	C17-C22	1.37 (1)	1.36 (2)	C21-C22	1.41 (1)	1.39 (2)
Fe2-C23	2.033 (8)	2.03 (1)	Fe2-C24	2.060 (9)	2.05 (1)	C23-C24	1.40 (1)	1.39 (2)
Fe2-C25	2.032 (8)	2.02 (1)	C24-C25	1.41 (1)	1.37 (2)	Fe2-C26	2.052 (7)	2.05 (1)
C25-C26	1.40 (1)	1.41 (2)	Fe2-C27	2.041 (6)	2.04 (1)	C23-C27	1.41 (1)	1.40 (2)
C26-C27	1.43 (1)	1.43 (2)	C27-C28	1.50 (1)	1.509 (2)	C28-C29	1.51 (1)	1.53 (2)
C29-C30	1.38 (1)	1.42 (2)	C30-C31	1.38 (1)	1.37 (2)	C31-C32	1.38 (2)	1.39 (2)
C32-C33	1.39 (2)	1.37 (3)	C29-C34	1.39 (1)	1.35 (2)	C33-C34	1.38 (2)	1.37 (3)

Angles

	198 K	298 K		198 K	298 K		198 K	298 K
F1-Sb-F2	89.4 (3)	89.1 (5)	F1-Sb-F3	89.5 (3)	89.4 (6)	F1-Sb-F4	179.4 (3)	179.5 (5)
F1-Sb-F5	89.1 (3)	89.0 (6)	F1-Sb-F6	89.8 (3)	90.4 (5)	F2-Sb-F3	90.7 (4)	90.9 (7)
F2-Sb-F4	90.3 (3)	90.9 (6)	F2-Sb-F5	87.9 (3)	177.4 (6)	F2-Sb-F6	177.1 (3)	92.2 (7)
F3-Sb-F4	91.0 (3)	90.9 (6)	F3-Sb-F5	178.0 (3)	177.4 (6)	F3-Sb-F6	92.1 (4)	92.2 (7)
F4-Sb-F5	90.4 (3)	90.7 (6)	F4-Sb-F6	90.5 (3)	90.0 (6)	F5-Sb-F6	89.3 (3)	89.8 (6)
C2-C1-C5	110.1 (7)	111 (1)	C1-C5-C6	127.4 (6)	126 (1)	C4-C5-C6	127.3 (7)	128 (1)
C1-C2-C3	107.3 (8)	108 (1)	C6-C6-C10	126.4 (7)	127 (1)	C7-C6-C10	107.1 (7)	107 (1)
C2-C3	108.6 (8)	108 (1)	C16-C17-C18	120.8 (8)	121 (1)	C14-C15-C16	124.6 (7)	126 (1)
C3-C4-C5	108.8 (7)	108 (1)	C17-C18-C19	120.8 (9)	121 (1)	C16-C17-C22	121.3 (8)	120 (2)
C1-C5-C4	105.1 (7)	105 (1)	C20-C21-C22	119.4 (9)	119 (1)	C18-C19-C20	120.4 (9)	120 (2)
C5-C6-C7	126.4 (7)	126 (1)	C15-C16-C17	110.0 (7)	111 (1)	C31-C32-C33	119 (1)	120 (2)
C6-C7-C8	108.7 (8)	108 (1)	C17-C22-C21	121.8 (8)	123 (1)	C30-C31-C32	119.9 (9)	118 (2)
C7-C8-C9	108.8 (8)	110 (1)	C18-C17-C22	117.8 (8)	117 (1)	C31-C32-C33	119 (1)	120 (2)
C8-C9-C10	108.4 (9)	108 (1)	C19-C20-C21	119.7 (9)	120 (1)			
C6-C10-C9	107.0 (8)	107 (1)	C24-C23-C27	109.5 (7)	109 (1)			
C12-C11-C15	106.5 (8)	107 (1)	C23-C24-C25	106.7 (8)	107 (1)			
C11-C12-C13	109.7 (8)	110 (1)	C24-C25-C26	109.8 (7)	111 (1)			
C12-C13-C14	107.1 (7)	106 (1)	C25-C26-C27	107.0 (7)	105 (1)			
C13-C14-C15	108.4 (7)	110 (1)	C23-C27-C28	126.4 (7)	126 (1)			
C11-C15-C16	126.9 (7)	127 (1)	C23-C27-C26	107.0 (7)	108 (1)			
C11-C15-C14	108.3 (7)	107 (1)	C27-C28-C29	110.8 (7)	111 (1)			
C26-C27-C28	126.6 (7)	126 (1)	C28-C29-C30	120.8 (7)	120 (1)			
C28-C29-C34	120.0 (7)	119 (1)	C29-C30-C31	121.5 (8)	121 (1)			
C29-C34-C33	119.4 (9)	118 (2)	C32-C33-C34	121 (1)	123 (2)			
			C30-C29-C34	119.1 (8)	121 (1)			

Complex **1** has a trans conformation as is found for most biferrocenes and mixed-valence biferrocenium cations. Only a few cis conformation biferrocenes are known,[15] and in all cases the molecule is held in a is conformation by a bridge between the 2,2″ positions of the fulvalene ligand. Dihedral angles between benzylcyclopentadienyl and fulvalenide rings at the metals is 0.7 (2)°. The fulvalenide ligand is planar with a dihedral angle of 0°. The fulvalenide dihedral angle varies from a crystallographically imposed 0° in some biferrocenium cations to 7.5 (5)° for biferrocenium tetrabromoferrate.[16]

A stereoview of the solid-state packing arrangement of 1′,1‴-dibenzylbiferrocene is available in the Supplementary Material.

Structure of 1′,1‴-Dibenzylbiferrocenium Hexafluoroantimonate (3). Complex **3** crystallizes in the monoclinic space group $P2_1$ at 298 K and retains this space group when cooled to 198 K. Final positional parameters for the 198 and the 298 K structures are available in the Supplementary Material. Selected bond distances and angles from the 198 and 298 K structures are given in Table IV. A perspective drawing of the 1′,1‴-dibenzylbiferrocenium cation from the 198 structure determination is shown in Figure 2. Though the cation has a trans conformation, the two benzyl substituents point in unusual directions away from the cation. This is the first reported case in which this occurs. The SbF_6^- anion is not disordered at either 198 or 298 K. In the case of the 198 K data, refinement of a disordered model which employed "idealized" SbF_6^- octahedra (Sb–F = 1.89 Å) to represent the anion density did *not* improve the fit of the data (R = 0.048 and R_w = 0.062). A comparison of the refinement parameters from the 198 and 298 K refinements shows that only the thermal parameters are affected by increasing the temperature. However, the increase in the fluorine thermal parameters is significantly larger than those for the other type of atoms (carbon, iron, and antimony). This suggests that though the SbF_6^- anions appear "ordered" at 298 K, they could in fact be tumbling in their lattice sockets, jumping between essentially indistinguishable orientations.

For complex **3** at 298 K the distances from the iron atom to the COM of the two rings are 1.69 (1) and 1.70 (1) Å for Fe(1) and 1.64 (1) and 1.65 (2) Å for Fe(2). At both metal atoms the

(15) Zhang, W.; Wilson, S. R.; Hendrickson, D. N. *Inorg. Chem.* **1989**, *28*, 4160 and references therein.

(16) Geib, S. J.; Rheingold, A. L.; Dong, T.-Y.; Hendrickson, D. N. *J. Organomet. Chem.* **1986**, *312*, 241.

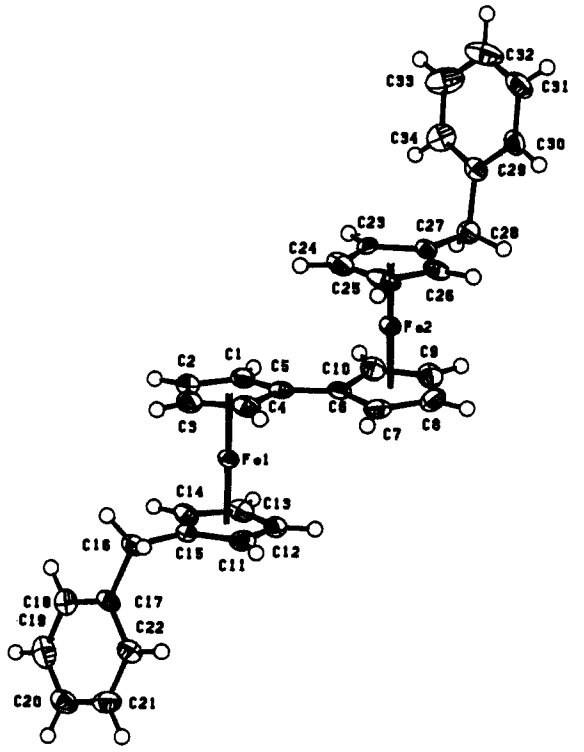

Figure 2. ORTEP drawing of the mixed-valence cation in 1′,1‴-dibenzylbiferrocenium hexafluoroantimonate (**3**) from the 198 K structure determination.

shorter distance is to the fulvalenide ring. At 198 K the Fe–COM distances are 1.692 (8) and 1.701 (8) Å for Fe(1) and 1.638 (9) and 1.65 (1) Å for Fe(2). Thus, the average Fe–COM distance for Fe(1) is marginally larger than that for Fe(2), which suggests that the Fe(1) site is the Fe^{III} ion in the mixed-valence cation. More definitive evidence for this assignment of valence states can be gleaned from the positioning of the SbF_6^- anion relative to the nearest cation. At 198 K the distance of Fe(1)–Sb is 5.471 (3) Å, whereas, the presumably Fe^{II} ion Fe(2) is situated so that Fe(2)–Sb = 5.833 (4) Å. This difference in electrostatic field due to the positioning of the anion would lead to an energy difference between the $Fe_a^{II}Fe_b^{III}$ and $Fe_a^{III}Fe_b^{II}$ vibronic states of the mixed-valence cation.

The fulvalenide dihedral angle for the cation in **3** is 6.8 (1)° at 298 K and increases to 7.0 (1)° at 198 K. Such an increase in dihedral angle upon a decrease in temperature could reduce the rate of tunneling (i.e., electron transfer) in the cation, for this rate depends on the tunneling matrix element (i.e., electronic coupling between Fe^{II} and Fe^{III} electronic manifolds).

Two other differences exist at the Fe(1) and Fe(2) halves of the cation. The dihedral angle between the two rings at Fe(1) is 4.2 (3)°, whereas it is only 2.0 (3)° at Fe(2) at 298 K. An even larger difference exists between the dihedral angles of phenyl group and attached cyclopentadienyl ring: 104.5 (5)° for Fe(1) and 73.6 (4)° for Fe(2) at 298 K. These angles do *not* change appreciably upon cooling **3** from 298 to 198 K. There seems to be several differences in Coulombic potentials and dihedral angles between the Fe(1) and Fe(2) metallocene moieties in the cation which would tend to valence trap complex **3**.

A stereoview of the solid-state structure of 1′,1‴-dibenzylbiferrocenium hexafluoroantimonate is shown in Figure 3. The packing arrangement consists of stacks of relatively large mixed-valence cations, with the SbF_6^- anions sandwiched between the stacks of cations.

Structure of 1′,1‴-Dibenzylbiferrocenium Hexafluorophosphate. Complex **2** crystallizes in the monoclinic space $C2/c$ at 296 K. Final positional parameters are available in the Supplementary Material; selected bond distances and angles are given in Table V. The mixed-valence cation sits on a center of inversion. A perspective drawing of this cation is shown in Figure 4. The

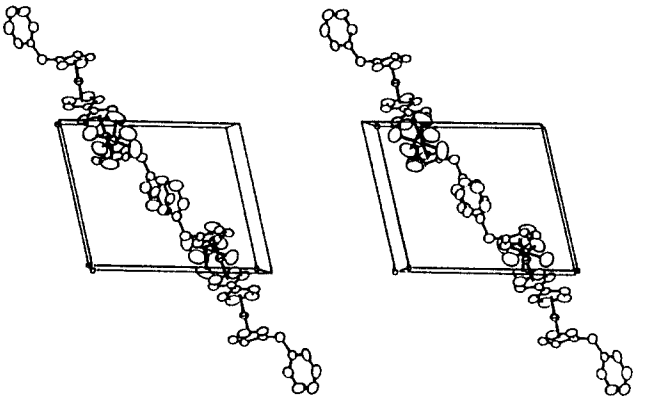

Figure 3. Stereoview of packing of 1′,1‴-dibenzylbiferrocenium hexafluoroantimonate (**3**) at 198 K.

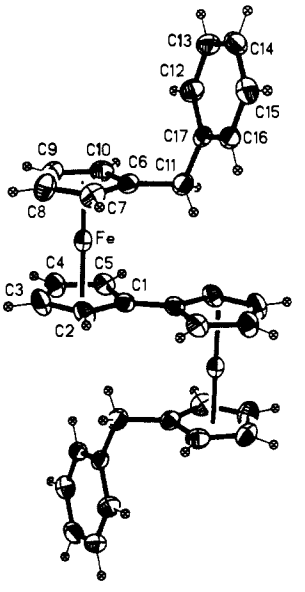

Figure 4. ORTEP drawing of the mixed-valence cation in 1′,1‴-dibenzylbiferrocenium hexafluorophosphate (**2**) at 296 K.

hexafluorophosphate anion was found to be disordered in two positions. Modeling with an octahedral PF_6^- group showed that the anion is disordered in two positions, one with an occupancy of 64% and the other an occupancy of 36%.

Since the mixed-valence cation in **2** is centrosymmetric, the dihedral angle in the fulvalenide ligand is exactly 0°. The two rings bonded to each iron ion are near to being coplanar with a dihedral angle of only 0.8 (3)°. The dihedral angle between the plane of the phenyl substituent and the cyclopentadienyl ring to which it is attached is 80.8 (3)°. Average distances from the iron atom to the rings carbon atoms are 2.067 (3) and 2.063 (3) Å for the benzylcyclopentadienyl and fulvalenide rings, respectively. These values are close to the average of the 2.075 (10) Å value for the ferrocenium cation[14] and the value of 2.033 (10) Å for ferrocene.[13] The distances from the iron atom to the COM of the two rings are 1.674 (4) Å for the fulvalenide ring and 1.669 (4) Å for the benzylcyclopentadienyl ring.

In contrast to the case for the SbF_6^- salt **3**, the two iron ions in the mixed-valence cation of the PF_6^- salt **2** are crystallographically equivalent. A stereoview of the packing of mixed-valence cations and the most populated orientation of the PF_6^- anions of complex **2** is shown in Figure 5. Complex **2** appears to be comprised of layers of mixed-valence cations with the relatively small PF_6^- anions sandwiched between the layers. In contrast to the case of the SbF_6^- salt, the PF_6^- anions of **2** are symmetrically disposed relative to the two iron ions in a given mixed-valence cation.

^{57}Fe Mössbauer Spectroscopy. Variable-temperature ^{57}Fe Mössbauer spectra were run for complexes **1**, **2**, and **3**. In the

Table V. Selected Bond Distances and Angles for 1′,1‴-Dibenzylbiferrocenium Hexafluorophosphate (2) at 296 K

		Distances	
Fe–C(1)	2.089 (4)	C(6)–C(10)	1.419 (6)
Fe–C(2)	2.060 (4)	C(6)–C(11)	1.501 (6)
Fe–C(3)	2.064 (5)	C(7)–C(8)	1.424 (7)
Fe–C(4)	2.058 (4)	C(8)–C(9)	1.387 (7)
Fe–C(5)	2.050 (4)	C(9)–C(10)	1.408 (7)
Fe–C(6)	2.086 (4)	C(11)–C(17)	1.512 (6)
Fe–C(7)	2.054 (4)	P–F(2′A)	1.503 (14)
Fe–C(8)	2.057 (5)	P–F(3′A)	1.596 (13)
Fe–C(9)	2.068 (5)	P–F(1)	1.573 (5)
Fe–C(10)	2.073 (4)	P–F(2)	1.570 (6)
C(1)–C(2)	1.435 (6)	P–F(3)	1.569 (6)
C(1)–C(5)	1.441 (6)	P–F(1′)	1.492 (10)
C(1)–C(1A)	1.431 (8)	P–F(2′)	1.503 (14)
C(2)–C(3)	1.411 (7)	P–F(3′)	1.596 (13)
C(3)–C(4)	1.415 (7)	P–F(1a)	1.573 (5)
C(4)–C(5)	1.402 (6)	P–F(2A)	1.570 (6)
C(6)–C(7)	1.429 (6)	P–F(3A)	1.569 (6)
		P–F(1′A)	1.492 (10)
		Angles	
C(2)–C(3)–C(4)	108.1 (4)	C(3)–C(4)–C(5)	108.7 (4)
C(1)–C(5)–C(4)	108.3 (4)	C(7)–C(6)–C(10)	107.2 (4)
C(7)–C(6)–C(11)	126.7 (4)	C(10)–C(6)–C(11)	126.0 (4)
C(6)–C(7)–C(8)	107.0 (4)	C(7)–C(8)–C(9)	109.0 (4)
C(8)–C(9)–C(10)	108.3 (4)	C(6)–C(10)–C(9)	108.5 (4)
C(6)–C(11)–C(17)	111.1 (4)	C(11)–C(17)–C(12)	119.9 (2)
C(11)–C(17)–C(16)	120.0 (2)	F(1)–P–F(2)	89.9 (3)
F(1)–P–F(3)	89.9 (3)	F(2)–P–F(3)	90.1 (4)
F(1)–P–F(1′)	55.4 (7)	F(2)–P–F(1′)	83.0 (5)
F(3)–P–F(1′)	35.4 (7)	F(1)–P–F(2′)	71.0 (5)
F(2)–P–F(2′)	31.4 (6)	F(3)–P–F(2′)	114.2 (6)
F(1′)–P–F(2′)	92.6 (7)	F(1)–P–F(3′)	134.5 (6)
F(2)–P–F(3′)	55.3 (5)	F(3)–P–F(3′)	64.8 (5)
F(1′)–P–F(3′)	88.9 (8)	F(2′)–P–F(3′)	85.2 (7)
F(1)–P–F(1A)	83.1 (4)	F(1′)–P–F(1A)	136.8 (7)
Fe–C(1)–C(5)	68.2 (2)	F(2)–P–F(1A)	86.2 (3)
C(2)–C(1)–C(5)	106.4 (3)	F(3)–P–F(1A)	172.0 (3)
C(2)–C(1)–C(1A)	127.4 (5)	F(2′)–P–F(1A)	60.0 (5)
C(5)–C(1)–C(1A)	125.9 (5)	F(3′)–P–F(1A)	118.1 (5)
F(1)–P–F(2A)	86.2 (3)	F(2)–P–F(2A)	174.8 (5)
C(1)–C(2)–C(3)	108.4 (4)	F(3)–P–F(2A)	93.4 (4)
F(1′)–P–F(2A)	97.6 (5)	F(3′)–P–F(3′A)	77.0 (9)
F(2′)–P–F(2A)	143.4 (6)	F(1A)–P–F(3′A)	134.5 (6)
F(3′)–P–F(2A)	129.8 (6)	F(2A)–P–F(3′A)	55.3 (5)
F(1A)–P–F(2A)	89.9 (3)	F(3A)–P–F(3′A)	64.9 (5)
F(1)–P–F(3A)	172.0 (3)	F(1′A)–P–F(3′A)	88.9 (8)
F(2)–P–F(3A)	93.3 (4)	F(2′A)–P–F(3′A)	85.2 (7)
F(3)–P–F(3A)	97.4 (5)	P–F(1)–F(1′)	59.4 (5)
F(1′)–P–F(3A)	132.3 (7)	P–F(1)–F(2′)	52.7 (5)
F(2′)–P–F(3A)	108.6 (6)	F(1′)–F(1)–F(2′)	83.9 (6)
F(3′)–P–F(3A)	52.6 (6)	P–F(1)–F(2′A)	57.7 (5)
F(1A)–P–F(3A)	89.9 (3)	F(1′)–F(1)–F(2′A)	95.5 (7)
F(2A)–P–F(3A)	90.1 (4)	F(2′)–F(1)–F(2′A)	97.6 (7)
F(1)–P–F(1′A)	136.8 (7)	P–F(2)–F(2′)	69.9 (10)
F(2)P–F(1′A)	97.6 (4)	P–F(2)–F(3′)	63.3 (6)
F(3)–P–F(1′A)	132.3 (7)	F(2′)–F(2)–F(3′)	129.2 (13)
F(1′)–P–F(1′A)	167.6 (14)	P–F(3)–F(1′)	67.8 (7)
F(2′)–P–F(1′A)	94.3 (7)	P–F(3)–F(3′)	58.4 (5)
F(3′)–P–F(1′A)	81.4 (8)	F(1′)–F(3)–F(3′)	107.1 (9)
F(1A)–P–F(1′A)	55.4 (7)	P–F(3)–F(3′A)	64.7 (6)
F(2A)–P–F(1′A)	83.0 (5)	F(1′)–F(3)–F(3′A)	117.9 (10)
F(3A)–P–F(1′A)	35.4 (7)	F(3′)–F(3)–F(3′A)	79.1 (8)
F(1)–P–F(2′A)	60.0 (5)	P–F(1′)–F(1)	65.2 (6)
F(2)–P–F(2′A)	143.4 (6)	P–F(1′)–F(3)	76.8 (9)
F(3)–P–F(2′A)	108.6 (6)	F(1)–F(1′)–F(3)	139.3 (11)
F(1′)–P–F(2′A)	94.3 (7)	P–F(2′)–F(1)	56.3 (5)
F(2′)–P–F(2′A)	113.0 (10)	P–F(2′)–F(2)	78.7 (11)
F(3′)–P–F(2′A)	161.3 (7)	F(1)–F(2′)–F(2)	110.3 (12)
F(1A)–P–F(2′A)	71.0 (5)	P–F(2′)–F(1A)	62.3 (6)
F(2A)–P–F(2′A)	31.4 (6)	F(1)–F(2′)–F(1A)	77.3 (7)
F(3A)–P–F(2′A)	114.2 (6)	F(2)–F(2′)–F(1A)	127.1 (14)
F(1′A)–P–F(2′A)	92.5 (7)	P–F(3′)–F(2)	61.4 (5)
F(1)–P–F(3′A)	118.1 (5)	P–F(3′)–F(3)	56.8 (5)
F(2)–P–F(3′A)	129.8 (6)	F(2)–F(3′)–F(3)	88.8 (7)
F(3)–P–F(3′A)	52.6 (6)	P–F(3′)–F(3A)	62.7 (6)
F(1′)–P–F(3′A)	81.4 (8)	F(2)–F(3′)–F(3A)	105.3 (9)
F(2′)–P–F(3′A)	161.3 (7)	F(3)–F(3′)–F(3A)	98.6 (8)

case of unoxidized 1′,1‴-dibenzylbiferrocene only a single quadrupole-split doublet is seen. Spectral features were least-squares fit to Lorentzian line shapes; fitting parameters are given in Table VI for complex **1**. The quadrupole splitting (ΔE_Q) and isomer shift (δ) for complex **1** are characteristic of a Fe^{II} metallocene.

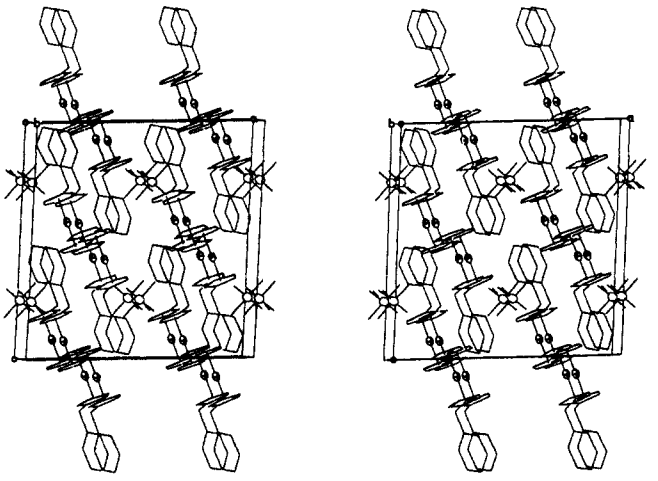

Figure 5. Stereoview of packing of 1′,1‴-dibenzylbiferrocenium hexafluorophosphate (2) at 296 K. Only one of the two orientations of the disordered anion is shown.

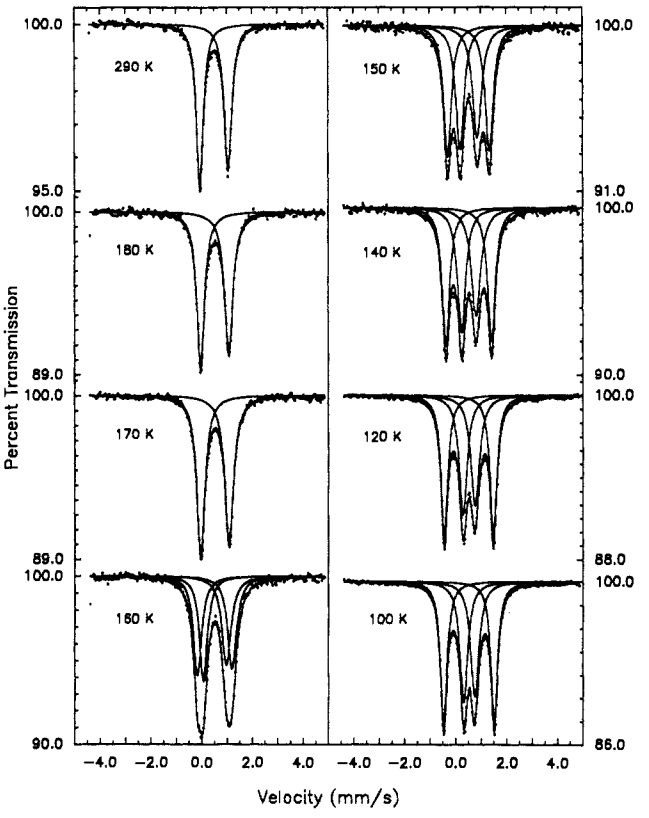

Figure 6. Variable-temperature ^{57}Fe Mössbauer spectrum for 1′,1‴-dibenzylbiferrocenium hexafluorophosphate (2).

Table VI. ^{57}Fe Mössbauer Spectral Fitting Parameters for Polycrystalline 1′,1‴-Dibenzylbiferrocene (1)

T, K	ΔE_Q, mm/s	δ,[a] mm/s	Γ,[b] mm/s
300	2.3495 (15)	0.4495 (8)	0.276 (2), 0.258 (3)
270	2.349 (12)	0.4439 (6)	0.274 (2), 0.258 (2)
240	2.358 (16)	0.4379 (8)	0.272 (3), 0.260 (3)
210	2.361 (14)	0.4362 (7)	0.284 (3), 0.270 (2)
180	2.368 (1)	0.4370 (5)	0.288 (2), 0.279 (2)
150	2.377 (12)	0.4334 (6)	0.286 (2), 0.278 (2)
120	2.371 (11)	0.4297 (5)	0.290 (2), 0.286 (2)

[a] Isomer shift relative to iron foil at room temperature. [b] Full width at half height taken from least-squares fitting program. The width for the line at more negative velocity is listed first for each doublet.

Table VII. ^{57}Fe Mössbauer Spectral Fitting Parameters for Polycrystalline 1′,1‴-Dibenzylbiferrocenium Hexafluorophosphate (**2**)

T, K	ΔE_Q, mm/s	δ,[a] mm/s	Γ,[b] mm/s	−ln (area)[c]
290	1.112 (2)	0.406 (1)	0.322 (3), 0.364 (4)	
280	1.108 (2)	0.405 (1)	0.322 (3), 0.360 (4)	
250	1.166 (3)	0.446 (2)	0.372 (4), 0.422 (6)	
240	1.145 (3)	0.413 (2)	0.334 (5), 0.378 (6)	−0.755
230	1.145 (3)	0.414 (2)	0.348 (4), 0.378 (5)	−0.843
220	1.121 (4)	0.409 (2)	0.348 (6), 0.388 (7)	−0.891
210	1.120 (2)	0.409 (1)	0.344 (3), 0.382 (4)	−0.975
200	1.117 (2)	0.407 (1)	0.354 (3), 0.398 (4)	−1.069
190	1.116 (3)	0.408 (1)	0.360 (4), 0.406 (4)	−1.127
180	1.114 (3)	0.406 (1)	0.366 (4), 0.404 (5)	−1.202
170	1.119 (2)	0.408 (1)	0.378 (3), 0.420 (4)	−1.278
160	0.909 (6)	0.404 (3)	0.370 (8), 0.438 (10)	−1.389
	1.363 (6)	0.399 (3)	0.390 (9), 0.420 (11)	
150	0.674 (6)	0.403 (3)	0.381 (9), 0.423 (11)	−1.502
	1.631 (6)	0.400 (3)	0.361 (8), 0.379 (9)	
140	0.569 (4)	0.410 (2)	0.348 (6), 0.438 (7)	−1.607
	1.782 (3)	0.405 (1)	0.348 (6), 0.358 (6)	
130	0.499 (3)	0.403 (3)	0.370 (5), 0.408 (5)	−1.665
	1.852 (2)	0.401 (3)	0.390 (4), 0.420 (7)	
120	0.472 (2)	0.412 (1)	0.324 (4), 0.378 (3)	−1.749
	1.920 (2)	0.403 (1)	0.320 (3), 0.410 (4)	
110	0.446 (9)	0.410 (5)	0.368 (3), 0.392 (3)	−1.816
	1.951 (7)	0.401 (4)	0.310 (2), 0.310 (2)	
100	0.430 (2)	0.414 (1)	0.368 (3), 0.388 (3)	−1.895
	1.976 (2)	0.402 (1)	0.312 (2), 0.314 (2)	

[a] Isomer shift relative to iron foil at room temperature. [b] Full width at half height taken from least-squares fitting program. The width for the line at more negative velocity is listed first for each doublet. [c] Minus the natural logarithm of the background-normalized spectral area.

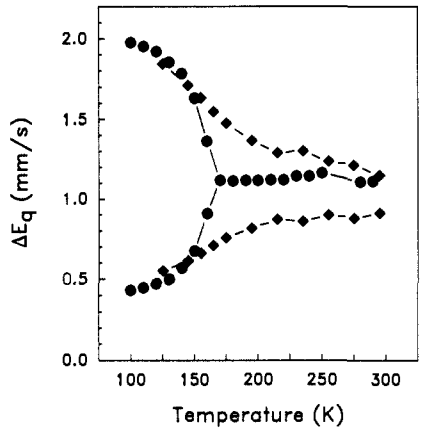

Figure 7. Plots of the quadrupole splitting, ΔE_Q, versus temperature evaluated by fitting the Mössbauer spectra of mixed-valence 1′,1‴-dibenzylbiferrocenium hexafluorophosphate (**2**) (filled circles) and 1′,1‴-dibenzylbiferrocenium hexafluoroantimonate (**3**) (filled diamonds). The lines are drawn just to guide the eyes.

Mössbauer spectra were run at 18 different temperatures in the range of 100–290 K for the PF_6^- complex **2**. Some of these spectra are illustrated in Figure 6; fitting parameters are collected in Table VII. Careful examination of these parameters shows that in the 100–170 K region complex **2** is converting from valence trapped to valence detrapped and this is completed by 170 K. That is, at low temperatures there are two doublets, one for a Fe^{III} site and the other for a Fe^{II} site. As the temperature is increased the components of the two doublets move together to become a single doublet above 170 K. In Figure 7 ΔE_Q for each of these two doublets is plotted versus temperature. At 170 K the valence-detrapped doublet has ΔE_Q = 1.119 (2) mm/s.

There are two interesting aspects of the temperature dependence of the Mössbauer spectra shown in Figure 6. First, the components of the two trapped-valence doublets just move together as the temperature is increased. There is very little line broadening evident in the averaging process. If intramolecular electron transfer in the cation of complex **2** were slow on the Mössbauer

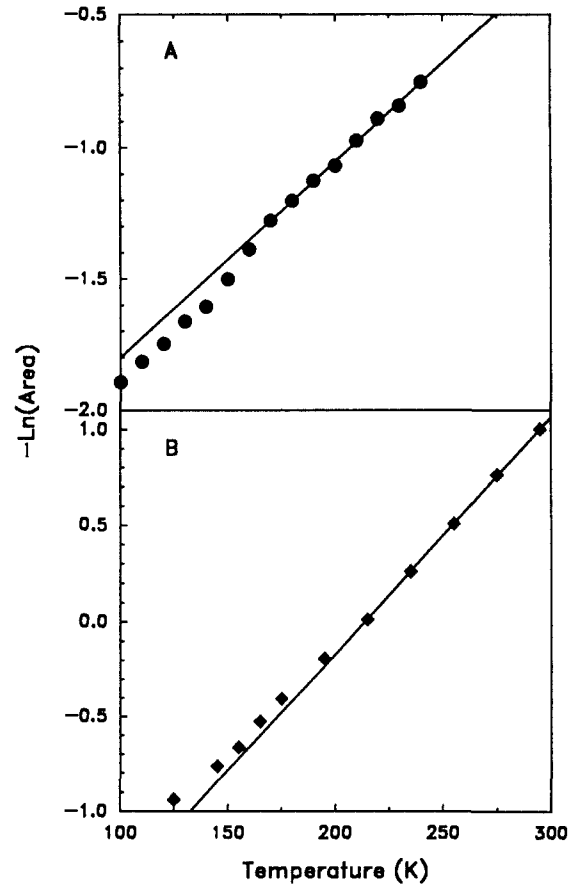

Figure 8. Plots of minus the natural logarithm of the background-normalized area of the Mössbauer spectrum, −ln (area), versus temperature for (A) 1′,1‴-dibenzylbiferrocenium hexafluorophosphate (**2**) and (B) 1′,1‴-dibenzylbiferrocenium hexafluoroantimonate (**3**). The straight lines result from least-squares fitting of data for complexes **2** and **3** in the high-temperature region.

time scale (i.e., rate $< \sim 10^6$ s^{-1}) at low temperature and then increased with increasing temperature, the rate should go through the range where coalescence effects would be seen. The line widths of the components of each doublet would be expected to broaden as the electron-transfer rate goes through the ^{57}Fe Mössbauer window (i.e., $\sim 10^6$ to $\sim 10^9$ s^{-1}). Thus, it has to be concluded that whatever process is leading to the averaging seen in Figure 6, it occurs at a rate which is at all temperatures fast relative to what the Mössbauer technique can sense. In a later section a description of the process which we believe is occurring will be given. Absence of line broadening in Mösbauer spectra has been noted[9a,b,c] for a few mixed-valence biferrocenes.

The second interesting feature of the spectra in Figure 6 relates to the temperature dependence of the recoilless fraction. The spectral area in each spectrum was integrated after correction for the background. In Figure 8A is given a plot of the negative of the natural logarithm of the spectral area, −ln (area), versus temperature. In terms of the Debye model for lattice vibrations the Mössbauer recoilless fraction f, which is proportional to the spectral area, has the dependence of $f = e^{-2W}$, where W is the Debye–Waller factor. In the high-temperature limit where the above spectra were run, $W = 3E_RT/k\theta_D^2$. The Debye temperature θ_D is a temperature which corresponds to some average lattice vibrational frequency, and E_R is the recoil energy of the ^{57}Fe atom. A plot of the logarithm of the Mössbauer spectral area versus temperature should give a straight line, the slope of which reflects the Debye temperature. In Figure 8A the plot of −ln (area) versus temperature does show one straight line dependence below $\sim$150 K, whereas there is a second straight line dependence in evidence above $\sim$175 K. This indicates that there is a change in the state of the lattice vibrations around $\sim$170 K. This is interesting for it is at this temperature that the spectrum converts to one of a valence-detrapped species. The slopes of the two straight lines

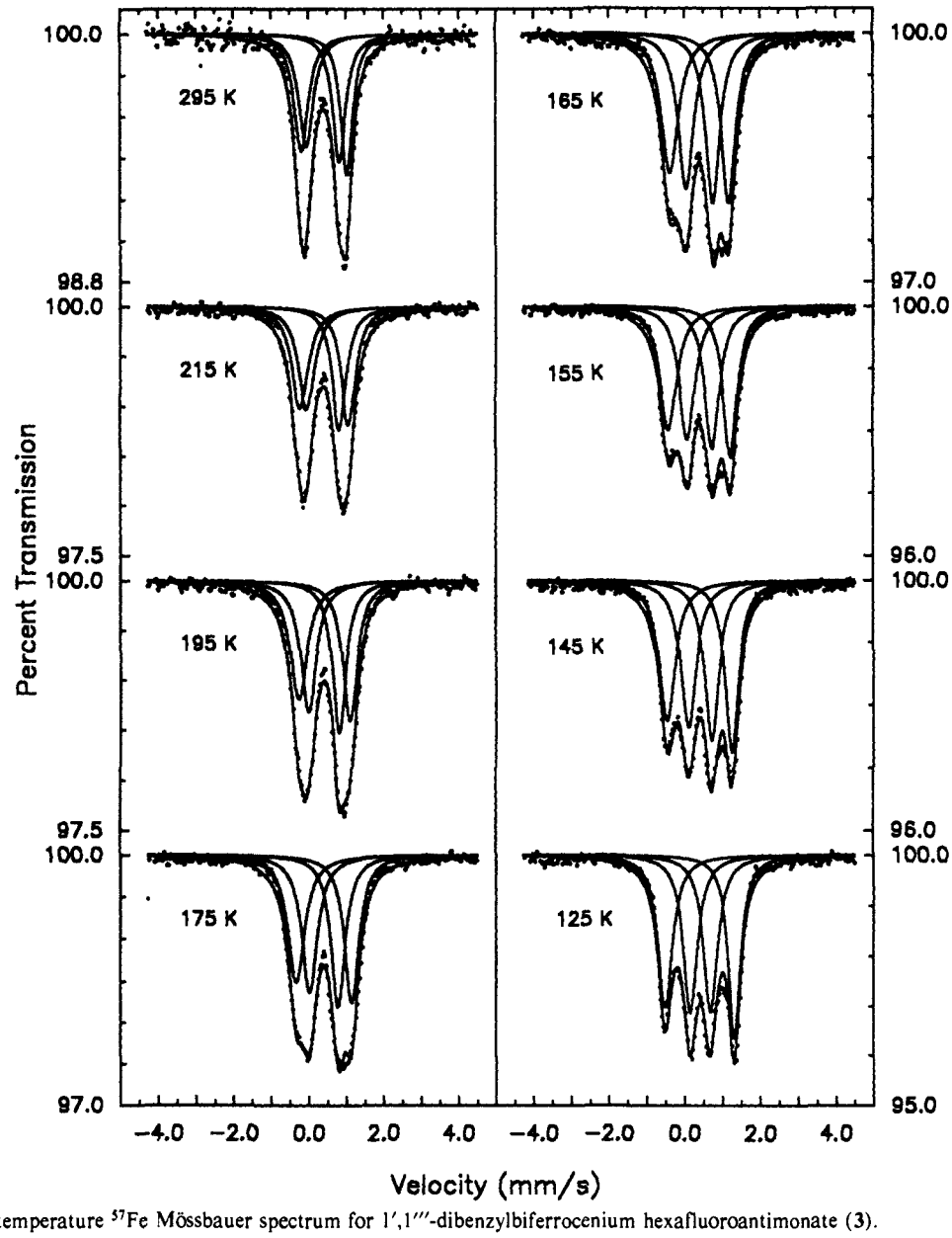

Figure 9. Variable-temperature ^{57}Fe Mössbauer spectrum for 1′,1‴-dibenzylbiferrocenium hexafluoroantimonate (**3**).

in Figure 8 are not very different, thus the Debye temperature does *not* change appreciably at ~170 K. However, the recoiless fraction falls off relatively abruptly at ~170 K. This indicates the onset of some cooperative process. Similar changes in −ln (area) versus temperature plots have been noted for other compounds. Frequently a phase transition is found to be the origin of a break in the −ln (area) versus temperature plot. In the case of complex **2** we suggest that at ~170 K the PF_6^- anions convert from being static to being dynamic. The disorder of the PF_6^- anions found in the 296 K structure could reflect a dynamic disorder in the PF_6^- anions, where at each lattice site the PF_6^- anion is jumping rapidly between two orientations. The onset of such motion in the PF_6^- anions could reduce the recoilless fraction for the mixed-valence cations. Preliminary results[17] of a solid-state ^{19}F NMR study for a *fixed* polycrystalline sample of complex **2** also suggest that the PF_6^- anions are dynamic at high temperature but become static at ~125 K (chemical shift anisotropy).

^{57}Fe Mössbauer spectra were collected at 11 different temperatures for the SbF_6^- complex **3**. In Figure 9 it can be seen that this mixed-valence compound also converts from valence trapped to valence detrapped as the temperature is increased. Fitting parameters are given in Table VIII. Visual inspection of the spectra in Figure 9 compared to those in Figure 6 show that the temperature dependencies are qualitatively similar. However, there are differences. The percent transmission is less for SbF_6^- complex **3** compared to the PF_6^- complex **2**. Also, the lines are broader for the SbF_6^- salt. As can be seen in Figure 9 it is possible to fit the 125 K spectrum to two doublets in an area ratio of 1:1. This is a trapped-valence spectrum with Fe^{II} and Fe^{III} signals. The line widths for these two doublets at 125 K are somewhat larger than for the two 120 K doublets in the spectrum of the PF_6^- salt (average line widths of 0.440 and 0.358 mm/s, respectively).

It is possible to fit the 295 K spectrum for the SbF_6^- salt to one doublet, however, the line widths for the two components are just too large to be reasonable. The 298 K structure of complex **3** shows two crystallographically different iron ions in the mixed-valence cation. As a result, we decided to fit the 295 K spectrum to two doublets, where the area ratio of the two doublets was held constant at 1:1. Thus, at each temperature throughout the 125–295 K region the spectrum for complex **3** was fit to two equal-area doublets. In Figure 7 is given a plot of the values of ΔE_Q versus temperature for these two doublets. It can be seen that there is a convergence of the ΔE_Q value for the two doublets, but in contrast to the case for complex **2** the two doublets for **3** do *not* become a single average-valence doublet. This is in agreement with the 198 and 298 K structures of complex **3**. It

(17) Webb, R. J.; Wittebort, R. J.; Hendrickson, D. N. Manuscript in preparation.

Table VIII. ^{57}Fe Mössbauer Spectral Fitting Parameters for Polycrystalline 1′,1‴-Dibenzylbiferrocenium Hexafluoroantiomonate (**3**)

T, K	ΔE_Q, mm/s	δ,[a] mm/s	Γ,[b] mm/s	−ln (area)[c]
295	1.15 (3)	0.45 (16)	0.40 (8), 0.40 (3)	1.0006
	0.91 (2)	0.38 (11)	0.40 (4), 0.41 (2)	
275	1.215 (18)	0.430 (9)	0.45 (3), 0.37 (2)	0.7604
	0.879 (20)	0.397 (1)	0.47 (3), 0.41 (2)	
255	1.237 (15)	0.420 (8)	0.44 (2), 0.41 (2)	0.5074
	0.899 (18)	0.405 (9)	0.51 (3), 0.44 (2)	
235	1.30 (2)	0.418 (12)	0.48 (4), 0.40 (3)	0.2604
	0.86 (2)	0.411 (12)	0.45 (4), 0.41 (3)	
215	1.29 (2)	0.426 (6)	0.53 (2), 0.52 (2)	0.0120
	0.87 (3)	0.391 (7)	0.436 (12), 0.452 (14)	
195	1.366 (9)	0.423 (4)	0.552 (16), 0.468 (12)	−0.1915
	0.818 (8)	0.409 (4)	0.498 (14), 0.432 (10)	
175	1.476 (8)	0.414 (4)	0.540 (15), 0.464 (12)	−0.4054
	0.756 (7)	0.409 (4)	0.500 (13), 0.450 (11)	
165	1.550 (7)	0.407 (4)	0.548 (14), 0.450 (10)	−0.5276
	0.707 (6)	0.414 (3)	0.494 (12); 0.450 (10)	
155	1.632 (6)	0.407 (3)	0.532 (12), 0.436 (9)	−0.6651
	0.660 (6)	0.417 (3)	0.496 (11), 0.462 (10)	
145	1.710 (6)	0.404 (3)	0.520 (11), 0.416 (8)	−0.7657
	0.613 (6)	0.421 (3)	0.496 (11), 0.456 (5)	
125	1.842 (5)	0.406 (3)	0.422 (11), 0.352 (9)	−0.9389
	0.551 (6)	0.427 (3)	0.490 (14), 0.494 (14)	

[a] Isomer shift relative to iron foil at room temperature. [b] Full width at half height taken from least-squares fitting program. The width for the line at more negative velocity is listed first for each doublet. [c] Minus the natural logarithm of the background-normalized spectral area.

is clear that the mixed-valence cations in the SbF_6^- complex become valence detrapped above ~215 K. However, because the environment (anion placement as well as phenyl substituent orientation) does *not* become the same for the two iron ions in each cation, two doublets are still seen above the valence-detrapping temperature. Each cation in complex **3** is interconverting rapidly on the Moössbauer time scale between its two vibronic states, symbolically described as $Fe_a^{II}Fe_b^{III}$ and $Fe_a^{III}Fe_b^{II}$. However, these two states are at different energies and have different average quadrupolar splittings. The fitting of the 295 K spectrum illustrated in Figure 9 was carried out while holding the area ratios of the two doublets to be 1:1. This means that instantaneously on the Mössbauer time scale we have equal amounts of cations in the two vibronic states, which also means that the difference in zero-point energies between the two vibronic states is small relative to kT in the ~200–295 K region.

The 295 K spectrum in Figure 9 was also fit to two doublets which do *not* have the same area. A comparably good fit was obtained with two doublets in an area of 1.36:1. It is, of course, difficult to pick between the two fittings. The latter fit with unequal areas could reflect different amounts of complexes in the two vibronic states. Such a Boltzmann distribution would reflect a difference in zero-point energies of the two states which is larger than kT in the 200–295 K region.

The fact that something is happening to the SbF_6^- complex **3** at ~200 K is clear from the −ln (area) versus temperature plot shown in Figure 9B. There is a change from one straight line to a second straight line behavior occurring at ~200 K. Again, it could be suggested that there is an onset of tumbling of the SbF_6^- anions at ~200 K. The thermal parameters for the SbF_6^- anions at 298 K, compared to those at 198 K, do support this. In contrast to the situation of the PF_6^- anions in complex **2**, the SbF_6^- anions in **3** seem to experience only one orientation in the lattice. If they are jumping above ~200 K, the SbF_6^- anions jump between relatively indistinguishable lattice sites. A comparison of −ln (area) versus temperature plots for complexes **2** and **3** (Figure 8) shows that the two salts experience different changes in recoilless fractions. As the temperature is increased, SbF_6^- complex **3** experiences an increase in recoilless fraction above a temperature of ~200 K. This can be rationalized, for in contrast to static PF_6^- anions, static SbF_6^- anions will absorb an appreciable amount of the 14.4 keV γ-rays. Thus, when the SbF_6^- anions start tumbling,

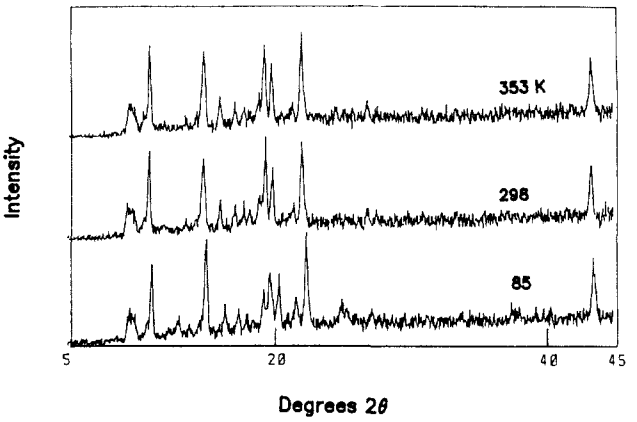

Figure 10. Temperature dependence of powder X-ray diffraction pattern for polycrystalline sample of 1′,1‴-dibenzylbiferrocenium hexafluorophosphate (**2**).

the recoilless fraction of complex **3** increases because the tumbling SbF_6^- anions cannot as readily absorb γ-rays.

Powder X-ray Diffraction. Since Mössbauer data show that the PF_6^- complex **2** converts from trapped to detrapped as the temperature is increased and only the 296 K X-ray structure is available, variable-temperature powder X-ray diffraction data were collected for complex **2**, see Figure 10. Powder patterns were collected at three different temperatures. As can be seen, there are only gradual changes in peak positions and intensities with changes in the temperature. The only conclusion which can be made is that if there is a structural change occurring it is a subtle change. A first-order phase transition between phases having a supergroup–subgroup interrelationship where subtle differences in diffraction characteristics occur may be a possibility.

Powder XRD patterns were also run for SbF_6^- complex **3** (figure available in Supplementary Material) at 77, 100, 200, 300, and 350 K. There are only gradual shifts in peak positions and intensities. There is no evidence for a dramatic change in structure.

IR and EPR Spectra. An application of infrared and electron paramagnetic resonance techniques to the study of mixed-valence complexes can give insight about time scale and electronic interaction factors related to the rate of intramolecular electron transfer. For mixed-valence biferrocene compounds IR spectroscopy has been shown[18] to be useful to tell whether or not a given compound is electronically delocalized or not. The electronic coupling between d-manifolds on the two metal centers in an electronically delocalized species is so large that there is no potential-energy barrier for electron transfer. The single unpaired electron in a "$Fe^{II}Fe^{III}$" biferrocene is in this case in a molecular orbital which is extensively delocalized over both metallocene units. There is no process involving electron transfer.

For the more interesting case where there is a potential-energy barrier for electron transfer, a mixed-valence biferrocene can be viewed on the short time scale of IR spectroscopy as being made up of two halves. If there is a vibrational mode which is sensitive to metal oxidation state, then two bands will appear in the IR spectrum. One band will be seen for the Fe^{II} metallocene unit and one band for the Fe^{III} metallocene unit. It has been shown[18] that the cyclopentadienyl perpendicular C–H bending vibration is most diagnostic of the oxidation state of iron metallocenes. This band is seen at 815 cm^{-1} for ferrocene and at 851 cm^{-1} for ferrocenium triiodide.

Unfortunately, the IR spectrum of the PF_6^- complex **2** is uninformative, for the PF_6^- anion has an intense and broad band in the 800–850-cm^{-1} region. However, this spectral region in the IR spectrum of the SbF_6^- complex **3** is free of SbF_6^- bands. In fact, two metallocene bands are seen at 822 and 855 cm^{-1} at room temperature. The SbF_6^- complex **3** does have a barrier for electron transfer. The temperature dependence seen in the Mössbauer spectrum for this complex is due to valence detrapping on the

(18) Kramer, J. A.; Hendrickson, D. N. *Inorg. Chem.* **1980**, *19*, 3330.

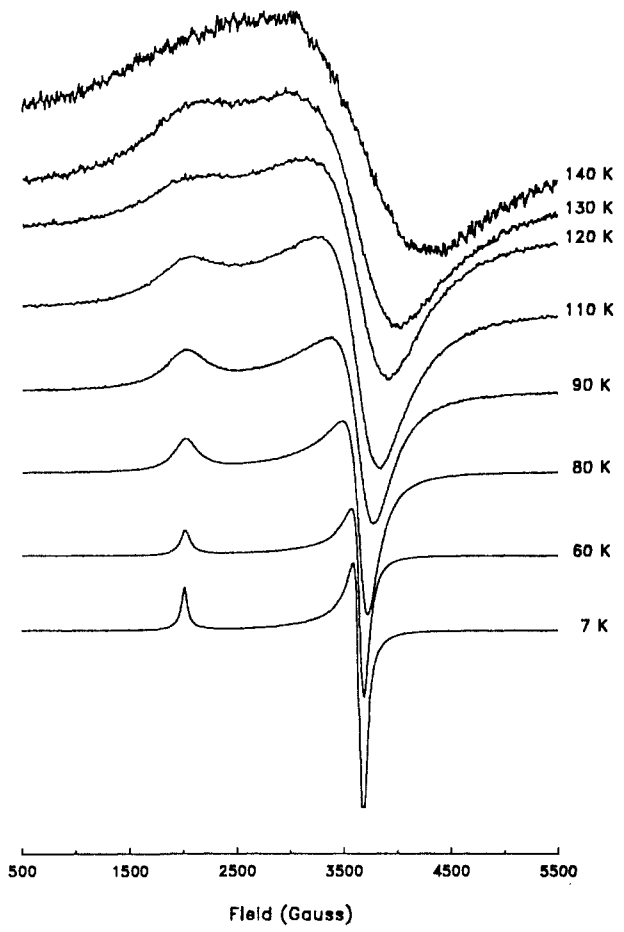

Figure 11. Temperature dependence of X-band EPR spectrum of a polycrystalline sample of 1′,1‴-dibenzylbiferrocenium hexafluoroantimonate (**3**).

Mössbauer time scale. Simply, this means that in a certain temperature region something happens in the solid, and *effectively* each mixed-valence cation is then interconverting rapidly between its two vibronic states. It may do this either by tunneling from a vibrational level of one state to a vibrational level of the other vibronic state or by becoming thermally activated to go over the barrier. The complex does not, however, become electronically delocalized at high temperatures.

Electronically localized Fe^{III} metallocenes generally give EPR signals only at low temperatures.[9d,19] The orbital angular momentum in the ground state leads to appreciable g tensor anisotropy, $\Delta g = g_{\parallel} - g_{\perp}$. For example, ferrocenium triiodide gives an axial EPR spectrum at 20 K which has signals at $g_{\parallel} = 4.35$ and $g_{\perp} = 1.26$ ($\Delta g = 3.09$). Mixed-valence biferrocenes that either have delocalized electronic structures with no potential-energy barrier or have an intramolecular electron-transfer rate in excess of the EPR time scale have been found[9d] to have Δg values less than ~0.8. This is a reflection of considerably reduced orbital angular momentum in the ground state which results from admixture of the S = 0 Fe^{II} description into the ground state. Recently it has been reported[20] that mixed-valence biferrocenes which valence detrap have Δg values in the range of ~1.1 to ~1.4. Anisotropies greater than this are found for those complexes which remain valence trapped at all temperatures.

In Figure 11 the temperature dependence of the X-band EPR spectrum of a polycrystalline sample of the SbF_6^- complex **3** is shown. The same sample which was used for the Mössbuaer experiments was used for the EPR study. At 7 K a typical axial powder pattern is seen with $g_{\parallel} = 3.35$ and $g_{\perp} = 1.86$, where $\Delta g = 1.49$ This same sample does valence detrap on the Mössbauer time scale (Figure 6). As the temperature of complex **3** is increased the $g_{\parallel}$ and $g_{\perp}$ signals in the EPR spectrum broaden considerably and the EPR signal disappears above ~150 K. In Table IX are collected g values for complex **3** and other related

(19) (a) Anderson, S. E.; Rai, R. *Chem. Phys.* **1973**, *2*, 216. (b) Sohn, Y. S.; Hendrickson, D. N.; Gray, H. B. *J. Am. Chem. Soc.* **1971**, *93*, 3603.
(20) Nakashima, S.; Masuda, Y.; Motoyama, I.; Sano, H. *Bull. Chem. Soc. Jpn.* **1987**, *60*, 1673.

Table IX. Variable-Temperature X-band EPR Results for Polycrystalline Samples of 1′,1‴-Dibenzylbiferrocenium Hexafluorophosphate (**2**) and 1′,1‴-Dibenzylbiferrocenium Hexafluoroantiomonate (**3**)

compd	temp (K)	$g_{\parallel}$	$g_{\perp}$	g_{HT}	Δg
2	7	3.36	1.83		1.53
	10	3.38	1.83		1.55
	20	3.37	1.83		1.54
	40	3.36	1.83		1.53
	60	3.35	1.83		1.53
	85	3.32	1.83	2.07	1.50
	95	3.33	1.86	2.07	1.47
	100	3.37	1.87	2.10	1.50
	110	3.33	1.89	2.10	1.44
	150			2.00	
	200			2.01	
	250			2.01	
	295			2.00	
3	7	3.35	1.86		1.50
	20	3.36	1.85		1.51
	40	3.35	1.85		1.50
	60	3.34	1.86		1.49
	80	3.33	1.87		1.46
	90	3.32	1.89		1.43
	110	3.27	1.91		1.36
	120	3.17	1.91		1.26
	130	3.08	1.91		1.17
	140			2.00	

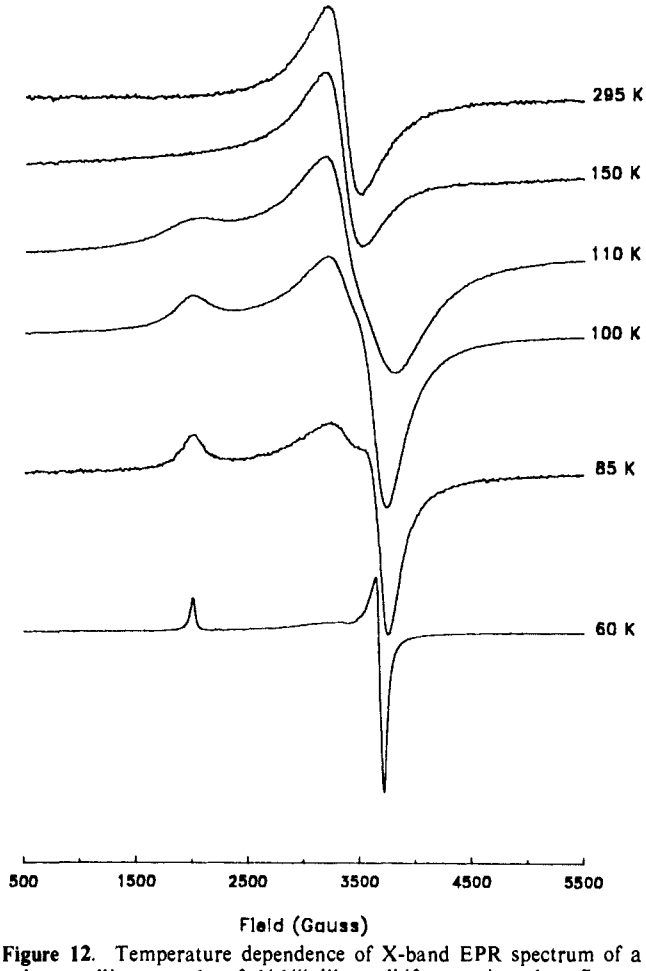

Figure 12. Temperature dependence of X-band EPR spectrum of a polycrystalline sample of 1′,1‴-dibenzylbiferrocenium hexafluorophosphate (**2**).

complexes. There are small shifts in $g_\parallel$ and $g_\perp$ features with changes in temperature for **3**; for example, at 110 K $g_\parallel = 3.27$ and $g_\perp = 1.91$.

There is one significant difference between the EPR characteristics of PF_6^- complex **2** and to those of complex **3**. The temperature dependence of the EPR spectrum for a polycrystalline sample of complex **2** is shown in Figure 12. As with complex **3** there is at 7 K an axial pattern observed for complex **2** with $g_\parallel = 3.36$ and $g_\perp = 1.83$. These $g_\parallel$ and $g_\perp$ signals broaden as the temperature of **2** is increased and eventually disappear above ~110 K. In contrast to the case of SbF_6^- complex **3**, further increases in the temperature of the PF_6^- salt **2** lead to the appearance of a new EPR signal. This new signal appears as a single derivative feature with $g = 2.00$ at 150 K and does not change in appearance up to at least 295 K. Closer examination shows that this new signal is even present in the 60–110 K spectra, superimposed with the axial signal. The only other mixed-valence biferrocene for which such an isotropic signal has been reported[9c] is biferrocenium hexafluorophosphate. In this case a signal at $g = 2.07$ is the only signal in the spectrum above ~140 K. At lower temperatures biferrocenium hexafluorophosphate shows an axial EPR signal with $g_\parallel = 2.65$ and $g_\perp = 1.86$. The Mössbauer spectrum for this same PF_6^- salt was reported[9b] to be a superposition of valence-trapped and valence-detrapped signals from 355 K down to 110 K.

The origin of the relatively isotropic high-temperature EPR signal for the two PF_6^- salts is *not* known. One possibility is that this signal arises from electron exchange between mixed-valence cations. At low temperatures each mixed-valence cation is valence trapped. *Inter*molecular magnetic exchange interactions between Fe^{III} ions in two neighboring cations, as perhaps propagated by a PF_6^- anion, may be relatively weak. Thus, the frequency of electron exchange could be less than would affect an X-band spectrum. When the temperature is increased, each cation becomes valence detrapped. The "extra" electron is rapidly transferring between the two iron ions in a given cation. Under these conditions *inter*molecular $Fe^{III}\cdots Fe^{III}$ magnetic exchange interactions may become more probable. If this *inter*molecular interaction becomes large enough, then the frequency of electron exchange between cations would exceed the X-band EPR frequency (~9 GHz). The $g_\parallel$ and $g_\perp$ signals would become exchange averaged to give an average signal. Whether this occurs in a given salt is a complicated function of the temperature dependence of the spin–lattice relaxation time which tends to broaden the $g_\parallel$ and $g_\perp$ signals as the temperature is increased, played off against the temperature dependence of the spin–spin relaxation due to electron exchange.

Another possible origin for the isotropic high-temperature EPR signal could be the onset of rapid electron transfer between cations. For complex **2** or biferrocenium hexafluorophosphate there are no data available which give insight about this possibility. Four-probe single-crystal electrical conductivity measurements have been carried out for biferrocenium triiodide.[21] This compound was found to be a semiconductor, where a plot of the logarithm of the conductivity versus temperature gave an activation energy of ~1000 cm^{-1}. If the activation energy for electrical conduction in complex **2** is of this magnitude or larger, then intermolecular electron transfer which affects the EPR spectrum is *not* being seen at ~140 K (kT ~84 cm^{-1}). Further study of the isotropic high-temperature EPR signal seen for the two PF_6^- salts is necessary to understand the nature of this signal.

Discussion

Micromodulation of Rate of Intramolecular Electron Transfer. In this paper the PF_6^- and SbF_6^- salts of the mixed-valence 1′,1‴-dibenzylbiferrocenium cation are described in detail. Onset of valence detrapping begins above ~100 K for the PF_6^- salt **2**, and by 170 K there is only one doublet in the Mössbauer spectrum. For the SbF_6^- complex **3** the Mössbauer spectrum shows an onset of valence detrapping in the 120–150 K range, and above ~200–250 K the SbF_6^- complex is completely valence detrapped. The I_3^- salt of this same cation has been reported[9c] to show an onset of valence detrapping above ~200 K, with complete detrapping and a single Mössbauer doublet at 270 K. Thus, in changing from the PF_6^- anion to the I_3^- anion for the 1′,1‴-dibenzylbiferrocenium cation there is a change from 170 to 270 K for the temperature where complete valence detrapping is seen. This is an appreciable change; however, it is not the most pronounced anion dependence we have seen. Very recently we communicated[22] that changing from I_3^- to PF_6^- for the 1′,1‴-diiodobiferrocenium counteranion leads to a change from valence detrapped (one Mössbauer doublet) at 4.2 K for the I_3^- salt to valence trapped at 350 K (two doublets) on the Mössbauer time scale.

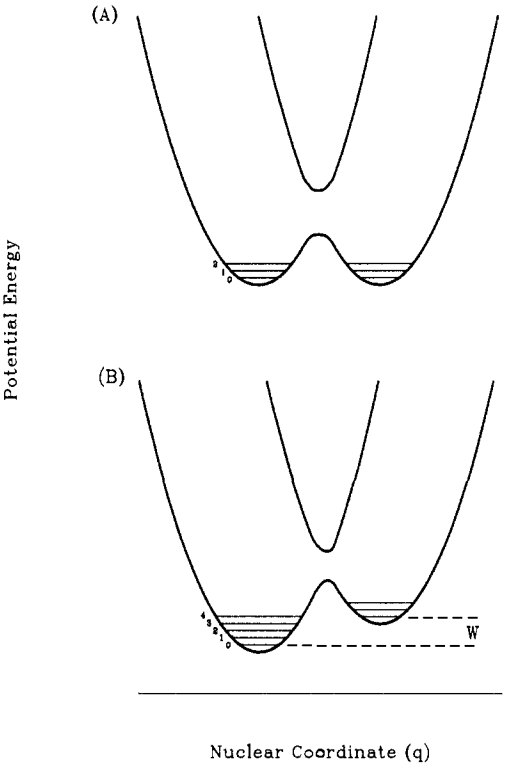

Figure 13. Potential energy plotted as a function of the out-of-phase combination of the two symmetric metal-ligand breathing vibrational modes on the two halves of a binuclear mixed-valence species. Diagram A is for the symmetric mixed-valence complex in the absence of environmental effects. Diagram B results if the environment about the binuclear mixed-valence complex is asymmetric. Vibrational levels are indicated.

The influence of the anion on the temperature at which valence detrapping occurs for a mixed-valence biferrocenium cation is easy to understand by reference to Figure 13. The coulombic potential experienced by a given mixed-valence cation is determined by the positioning of nearby anions and cations in the crystal lattice. If the two iron ions in the cation are crystallographically equivalent, then the potential-energy diagram for the ground state of the cation is symmetric as pictured on Figure 13A. The two vibronic states, $Fe_a^{II}Fe_b^{III}$ and $Fe_a^{III}Fe_b^{II}$, are at the same energy. It is easy for the mixed-valence cation to tunnel back and forth between its two states at a rate greatly in excess of the upper value (~10^9 s^{-1}) that can be sensed by the Mössbauer technique. The cations in some salts are even tunneling this fast at 4.2 K.[9d] If the crystal potential is inequivalent for the two iron ions in a given cation, then the potential-energy diagram shown in Figure 13B is obtained. The positioning of nearby anions (and cations) leads to a difference in energy of the two vibronic states. The cation tends to become valence trapped in one of the two vibronic states. The positioning of counteranions can very dramatically affect the rate of tunneling

(21) Cohn, M. J.; Hendrickson, D. N. Unpublished results.

(22) Webb, R. J.; Rheingold, A. L.; Geib, S. J.; Staley, D. L.; Hendrickson, D. N. *Angew. Chem., Int. Ed. Engl.* **1989**, *28*, 1388.

of a mixed-valence cation from one vibronic state to the other. It is possible in solution that the sluggish motion of an anion near to an outer-sphere association of two redox-active cations could appreciably affect the rate of electron transfer (tunneling) between the two cationic complexes. Also, sluggish motion of the immediate solvent structure about a redox-active pair of complexes would be expected to slow down *inter*molecular electron transfer.

It is clear how a mixed-valence cation sitting in an asymmetric crystal lattice manages to become valence detrapped. As per Figure 13B, the cation in SbF_6^- complex **3** is at low temperatures trapped in the lower energy state. It is in the lowest energy vibrational level (level 0 in Figure 13B), which would be expected to have a relatively low rate of tunneling to any vibrational level of the higher energy state. However, upon an increase in the temperature cations in complex **3** thermally access higher energy vibrational levels (marked 1, 2, etc., in Figure 13B). Cations in these vibrational levels experience a greater probability for tunneling to the other vibronic state. This is the case for the probability functions for cations in these higher energy vibrational levels penetrate further into the potential-energy barrier, and the potential-energy barrier is narrower.

It is clear that tunneling is very important for intramolecular electron transfer in mixed-valence biferrocenium-type cations. After all, it has been reported[9] that salts of some of these cations, for example, 1′,1‴-diiodobiferrocenium triiodide, have rates in excess of the Mössbauer time scale (rate > 10^9 s^{-1}) even at 4.2 K. Such a fast rate of electron transfer at this low a temperature is only attributable to quantum mechanical tunneling. IR data[9] show that there is a barrier for electron transfer.

Finally, the possible origin of the absence of line broadening observed in the Mössbauer spectra of **2** and **3** (Figures 6 and 9, respectively) as the temperature of these two compounds is increased needs to be discussed. If the observed changes in Mössbauer spectrum (see Figure 6) were simply attributable to the mixed-valence cation changing from having a small rate of electron transfer to having a rate which is fast on the Mössbauer time scale, then there should be line broadening seen in the intermediate temperature region. As the rate of intramolecular electron transfer increases through the 10^6–10^9 s^{-1} rate range that the Mössbauer technique can sense, the lines in the spectrum should broaden and coalesce. This is not seen. It has to be concluded that whatever the process is which is leading to the temperature dependence seen in Figure 6 it has to be occurring at a rate which is fast on the Mössbauer time scale *at all temperatures*. It is quite likely that what is affecting the Mössbauer spectrum and imparting a temperature dependence is the onset of lattice dynamics in complexes **2** and **3**. At low temperatures (<100 K) all parts of the crystal lattices of these complexes will be static. As the temperature of a compound is increased the thermal energy could achieve the value necessary to trigger off a cooperative change in the crystal lattice. If the conversion from valence trapped to valence detrapped for complexes **2** and **3** occurs in a defect-affected (first-order?) phase transition, then a nucleation and growth mechanism[23] could be important. As the temperature is increased small regions (domains) of valence-detrapped species nucleate preferably at defect sites in a crystal which is comprised of large domains of valence-trapped species. In the nucleation and growth mechanism for phase transitions, there are two rates which can be influential. On the one hand there is a rate at which minority-phase domains (valence-detrapped species) of size large enough to persist nucleate in a sea of majority-phase species. After these critical-sized minority domains form, there is then a different rate, namely a rate at which the domain wall moves and the minority-phase domains grow considerably in size at the expense of the majority phase. Domain walls can probably move at a variety of rates. If there is good correlated motion of several mixed-valence cations in a crystal region, it is possible that the rate of domain wall movement would be fast, faster even than could be sensed by the ^{57}Fe Mössbauer technique. When the mixed-valence complex is in the "trapped domain", the cation experiences the asymmetric potential-energy diagram shown in Figure 13B. The tunneling rate is then very small for the cation. When it is in the "detrapped domain", the cation experiences the symmetric potential-energy diagram shown in Figure 13A. In this case the mixed-valence cation can tunnel very rapidly between its two vibronic states, and the rate of tunneling greatly exceeds the Mössbauer time scale. Thus, in observing the temperature dependence in the Mössbauer spectrum we are *not* directly seeing a mixed-valence cation tunnel between its two vibronic states. This tunneling rate is either very slow (Figure 13B) or very fast (Figure 13A) relative to the ^{57}Fe Mössbauer time scale. One feature which could be different between valence-trapped and valence-detrapped domains is the static or dynamic nature of the PF_6^- and SbF_6^- anions.

In complexes **2** and **3** where the mixed-valence cations are assembled in layers and stacks, respectively, it is possible that the domain wall movement involves solitons.[24] Solitons are nondispersive wave packets which move at a speed near to the speed of sound in solids. Such solitonic wave packets would move past a given lattice site at a rate much faster than the Mössbauer technique can sense.

Acknowledgment. We are grateful for funding from National Institutes of Health grant HL13652 (D.N.H.).

Supplementary Material Available: Figures showing variable-temperature powder XRD pattern for SbF_6^- complex **3**, the ORTEP drawing of the SbF_6^- anion in complex **3**, and the packing arrangement for complex **1** and complete tables of bond lengths and angles and thermal parameters for **1**, **2**, and **3** (23 pages); tables of observed and calculated structure factors for complex **1** at 296 K, **2** at 296 K, and **3** at 198 and 298 K (49 pages). Ordering information is given on any current masthead page.

(23) Rao, C. N. R.; Rao, K. J. *Phase Transitions in Solids*; McGraw-Hill: New York, 1978.
(24) Solitons, Vol. 17. Trullinger, S. E., Zakharov, V. E., Pokrovsky, V. L., Eds.; In series *Modern Problems in Condensed Matter Sciences*; Agranovich, V. M., Maradudin, A. A., Eds.; North Holland: Amsterdam, 1986.